# Electron-Acceptor Properties of Hypericin and Its Salts: An ESR/ENDOR and Electrochemical Study

**Fabian Gerson,*,† Georg Gescheidt,*,† Pascal Häring,† Yehuda Mazur,*,‡ Dalia Freeman,‡ Hubert Spreitzer,§ and Jörg Daub§**

*Contribution from the Institut für Physikalische Chemie der Universität, Klingelbergstrasse 80, CH-4056 Basel, Switzerland, Department of Organic Chemistry, The Weizmann Institute of Science, Rehovot 76100, Israel, and Institut für Organische Chemie der Universität, D-93040 Regensburg, Germany*

*Received July 3, 1995*[⊗]

**Abstract:** Hypericin (**HyH**) and its conjugate base $\mathbf{Hy}^-$ (existing as salts $\mathbf{Hy}^-\mathbf{X}^+$, where X = Na, Cs, $Et_3NH$, lysineH) undergo one-electron reduction to yield the radical anion $[\mathbf{HyH}]^{\bullet-}$ and the radical dianion $\mathbf{Hy}^{\bullet 2-}$, respectively, which have been investigated by ESR, ENDOR, and TRIPLE-resonance spectroscopy. Whereas $\mathbf{Hy}^{\bullet 2-}$ can be generated from $\mathbf{Hy}^-$ by electrolysis or by several reducing agents in a variety of solvents and is stable for weeks even at room temperature, the spectra of $[\mathbf{HyH}]^{\bullet-}$, produced from **HyH** with zinc in anhydrous *N,N*-dimethylformamide or with potassium in tetrahydrofuran, are replaced within a few minutes by those of $\mathbf{Hy}^{\bullet 2-}$. The hyperfine data for $[\mathbf{HyH}]^{\bullet-}$ and $\mathbf{Hy}^{\bullet 2-}$ are consistent with a helically twisted carbon framework of $C_2$ symmetry. A prominent hyperfine feature of $\mathbf{Hy}^{\bullet 2-}$ is a relatively large coupling constant of +0.167 mT due to a single proton situated on the 2-fold axis in a symmetric $C(3)-O^{\delta-}\cdots H\cdots{}^{\delta-}O-C(4)$ bridge. This value is missing for $[\mathbf{HyH}]^{\bullet-}$ which does not possess such a bridge but has two non-dissociated OH groups in the 3,4-positions. Cyclic voltammograms of hypericin salts ($\mathbf{Hy}^-\mathbf{X}^+$) exhibit up to three reversible reduction waves in the region −1.0 to −2.2 V (*vs* Ag/AgCl). They are attributed to the consecutive redox steps $\mathbf{Hy}^-/\mathbf{Hy}^{\bullet 2-}$, $\mathbf{Hy}^{\bullet 2-}/\mathbf{Hy}^{3-}$, and (presumably) $\mathbf{Hy}^{3-}/\mathbf{Hy}^{\bullet 4-}$. Analogous electrochemical studies of free hypericin (**HyH**) require the use of strictly anhydrous solvents, in which **HyH** is sufficiently soluble and the facile deprotonation to $\mathbf{Hy}^-$ can be avoided. Under these conditions, a wave attributed to reduction of a proton is observed at a less negative potential than that of $\mathbf{Hy}^-$ to $\mathbf{Hy}^{\bullet 2-}$, while the subsequent waves correspond to those of $\mathbf{Hy}^-\mathbf{X}^+$.

## Introduction

In order to account for pharmacological activity of drugs, several approaches are practicable. Most challenging is the search for mechanisms underlying various activities of one and the same compound. This is the case with hypericin which can be found in plants of the genus *hypericium*, most commonly in St. Johns wort.[1] Apart from causing hypericism, a light-dependent *in vivo* disease of grazing animals,[2] extracts of *hypericium* plant exhibit a vast palette of pharmacological activities and have been employed as antidepressive agents.[3] Moreover, hypericin isolated from plants and, likewise, the synthetic compound shows antitumoral[4] as well as marked antiviral activity and is being investigated as a potential antiviral drug, particularly against HIV.[5]

There is some dispute about the crucial role of light for the *in vivo* and *in vitro* activities of hypericin.[5,6] This quinoid molecule with an extended $\pi$-system can act as a photosensitizer and as an efficient electron acceptor. Whereas its function as a sensitizer in the photochemical production of singlet dioxygen and superoxide has been studied by several research groups,[7,8] its electron-accepting properties have received less attention.[8,9] It is noteworthy that the activity of hypericin also occurs with *exclusion of dioxygen* and in both the *presence and absence of light* but is promoted by irradiation and an increase in concentration (without irradiation).[10,11] These findings point to the uptake of an electron by hypericin, leading to the formation of semiquinone-type radicals. Such a process is favored by

† Universität Basel.

‡ The Weizmann Institute of Science.

§ Universität Regensburg.

⊗ Abstract published in *Advance ACS Abstracts,* November 1, 1995.

(1) Brockmann, H. V.; Falkenhausen, E. H.; Neeff, R.; Dorlars, A.; Budde, G. *Chem. Ber.* **1951**, *84*, 865−87.

(2) Duran, N.; Song, P. S. *Photochem. Photobiol.* **1986**, *43*, 677−80.

(3) Daniel, K. *Hippocrates* **1949**, *19*, 526. Muldner, H.; Zoller, M. *Arzneim. Forsch.* **1984**, *34*, 918−20. Suzuki, O.; Katsumata, Y.; Oya, M.; Bladt, S.; Wagner, H. *Planta Med.* **1984**, *50*, 272−4.

(4) Thomas, C.; Pardini, R. S. *Photochem. Photobiol.* **1992**, *55*, 831−7.

(5) Meruelo, D.; Degar, S.; Amari, N.; Mazur, Y.; Lavie, D.; Levin, B.; Lavie, G. In *Natural Products as Antiviral Agents*; Chu, C. K., Cuttre, H. G., Eds.; Plenum Press: New York, 1992; pp 91−119. Tang, J.; Colachino, J. M.; Larsen, S. H.; Spitzer, W. *Antiviral Res.* **1990**, *13*, 313−25. Moraleda, G.; Wu, T. T.; Jilbert, A. R.; Aldrich, C. E.; Condreay, L. D.; Larsen, S. H.; Tang, J. C.; Colacino, J. M.; Mason, W. S. *Antiviral Res.* **1993**, *20*, 235−47.

(6) Meruelo, D.; Lavie, G.; Lavie, D. *Proc. Natl. Acad. Sci. U.S.A.* **1988**, *85*, 5230−4. Lavie, G; Valentine, F.; Levin, B.; Mazur, Y.; Gallo, G.; Lavie, D.; Weiner, D.; Meruelo, D. *Proc. Natl. Acad. Sci. U.S.A.* **1989**, *86*, 5963−7. Degar, S.; Prince, A. M.; Pascual, D.; Lavie, G.; Levin, B.; Mazur, Y.; Lavie, D.; Ehrlich, L. S.; Carter, C.; Meruelo, D. *AIDS Res. Hum. Retroviruses* **1992**, *8*, 1929−36. Lenard, J.; Rabson, A.; Vanderoef, R. *Proc. Natl. Acad. Sci. U.S.A.* **1993**, *90*, 158−62.

(7) Jardon, P.; Lazortchak, N.; Gautron, R. *J. Chim. Phys.* **1987**, *84*, 1141−5. Racinet, H.; Jardon, P.; Gautron, R. J. *J. Chim. Phys.* **1988**, *85*, 971−7. Bouirig, H.; Eloy, D.; Jardon, P. *J. Chim. Phys.* **1992**, *89*, 1391−411. Senthil, V.; Longworth, J. W.; Ghiron, C. A.; Grossweiner, L. I. *Biochim. Biophys. Acta* **1992**, *1115*, 192−200. Thomas, C.; MacGill, R. S.; Miller, G. C.; Pardini, R. S. *Photochem. Photobiol.* **1992**, *55*, 47−53.Weiner, L.; Mazur, Y. *J. Chem. Soc., Perkin Trans. 2* **1992**, 1439−42. Gai, F.; Fehr, M. J.; Petrich, J. W. *J. Am. Chem. Soc.* **1993**, *115*, 3384−5. Diwu, Z.; Lown, J. W. *Free Radical Biol. Med.* **1993**, *14*, 209. Stevenson, N. R.; Lenard, J. *Antiviral Res.* **1993**, *21*, 119−27.

(8) Malkin, J.; Mazur, Y. *Photochem. Photobiol.* **1993**, *57*, 929−33.

(9) Redepenning, J.; Tao, N. *Photochem. Photobiol.* **1993**, *58*, 532−5.

(10) De Witte, P.; Agostinis, P.; Van Lint, J.; Merlevede, W.; Vandenheede, J. R. *Biochem. Pharmacol.* **1993**, *46*, 1929−36.

(11) Hudson, J. B.; Lopez-Bazzocchi, I.; Towers, G. H. N. *Antiviral Res.* **1991**, *15*, 101−12. Lopez-Bazzocchi I.; Hudson, J. B.; Towers, G. H. N. *Photochem. Photobiol.* **1991**, *54*, 95−8. Hudson, J. B.; Harris, L.; Towers, G. H. N. *Antiviral Res.* **1993**, *20*, 173−8.

0002-7863/95/1517-11861$09.00/0 

irradiation because the electron-accepting properties of molecules are greatly enhanced in the excited state.[12] Nevertheless, the final products, with or without light, should be the radicals in the electronic ground state. This behavior parallels that of structurally related anthracyclines.[13]

The structure of hypericin was established as a 7,14-diketonaphthodianthrone derivative ([7,14]**HyH**) by its total synthesis[14] and later confirmed by X-ray crystallographic analysis of its pyridinium complex.[15] However, the structure of the 1,6-diketo tautomer ([1,6]**HyH**) has been recently assigned to hypericin in the solid state or in dry non-protic solvents like tetrahydrofuran (THF), acetone, or ethyl acetate.[16] This tautomer exists in solution as an aggregate which is stabilized by self-association through intermolecular H-bonding. On dilution as well as on addition of water or protic solvents, the aggregate decomposes and [1,6]**HyH** isomerizes to [7,14]**HyH**, the stable monomeric form of hypericin. [1,6]**HyH** is more acidic than [7,14]**HyH** and both tautomers react with bases, to give monobasic salts $\mathbf{Hy}^{-}X^{+}$.

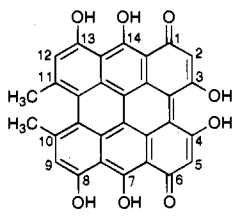

[1,6]HyH

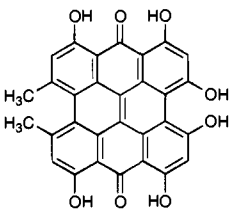

[7,14]HyH

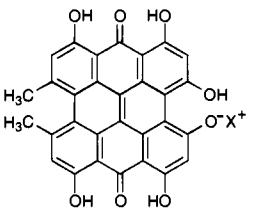

$Hy^{-}X^{+}$

X = Na, Cs, $Et_3NH$, lysineH

We have carried out one-electron reduction of **HyH** and its conjugate base $\mathbf{Hy}^{-}$ and characterized the thus generated semiquinone radical anion $[\mathbf{HyH}]^{\bullet -}$ and dianion $\mathbf{Hy}^{\bullet 2-}$ by their hyperfine data with the use of ESR, ENDOR, and TRIPLE-resonance spectroscopy. As both tautomers, [1,6]**HyH** and [7,14]**HyH**, possess the $C_2$ symmetry, they cannot be distinguished by the multiplicities of the hyperfine patterns due to sets of equivalent protons in the ESR spectra of $[\mathbf{HyH}]^{\bullet -}$. Therefore, the notation $[\mathbf{HyH}]^{\bullet -}$ does not specify either of the tautomers. However, considering the highly dilute solutions used in our studies (*ca.* $10^{-3}$ M), it is likely that the ESR spectrum of the radical anion arises from the 7,14-isomer and we have tentatively assigned the observed coupling constants to [7,14]$[\mathbf{HyH}]^{\bullet -}$. The reduction processes were followed by cyclic voltammetry under various conditions and were also monitored by electronic absorption spectroscopy.

## Experimental Section

**HyH** and its salts $\mathbf{Hy}^{-}X^{+}$ (X = Na, Cs, $Et_3NH$, lysineH) were prepared as described elsewhere.[14]

For ESR and ENDOR spectroscopy, **HyH** and $\mathbf{Hy}^{-}X^{+}$ were reduced with potassium in tetrahydrofuran (THF) and with zinc in *N,N*-dimethylformamide (DMF). In the case of $\mathbf{Hy}^{-}X^{+}$, reduction was also carried out with zinc in DMF/$H_2O$ and DMF-$d_8$/$D_2O$ (10:1) and electrolytically on a helical gold cathode[17] (counter electrode, platinum wire; solvent, DMF; supporting electrolyte, tetra-*n*-butylammonium perchlorate). ESR spectra were taken on a Varian-E9 instrument at 298 K, while a Bruker-ESP-300 system served for ENDOR and TRIPLE-resonance studies at 243 K. The saturation of an ESR line, as a prerequisite for a successful ENDOR experiment,[18] required a strikingly low microwave power (0.8 mW). The simulations of the ESR spectra made use of the proton-coupling constants derived from the positions of the ENDOR signals and refined by a fitting procedure.[19]

Cyclic voltammograms were recorded either in a one-compartment three-electrode cell, using a potentiostat AMEL 553, a function generator AMEL 568, and an on-line data processor ACER 910 [20] (Regensburg), or on a Metrohm Polarecord E 506 and a VA scanner E 612 with a VA stand 663 (Basel). The standard conditions were as follows: working electrode, platinum disk or hanging mercury drop; counter electrode, platinum wire or glassy carbon; calibration by the half-wave potential of ferrocene/ferrocene$^{\bullet +}$ and adaptation to Ag/AgCl as the reference;[21] solvent, acetonitrile (MeCN), MeCN/$H_2O$ (10:1), DMF, or THF; supporting electrolyte, tetra-*n*-butylammonium perchlorate or hexafluorophosphate (*n*-$Bu_4NClO_4$ or *n*-$Bu_4NPF_6$; 0.1 M); temperature, 298 K.

All solvents were of highest purity. For experiments with **HyH**, requiring the elimination of slightest traces of water, the solvents DMF and THF were refluxed over phosphorus pentoxide and sodium/potassium alloy, respectively. The supporting electrolyte was kept over night in high vacuum before use.

Simultaneous recording of the electronic absorption bands in the visible region was performed on a Perkin-Elmer Lambda 9 (Regensburg) and on a J&M TIDAS-16 instrument (Basel) which were attached to the three-electrode cell[22] and to an optical cavity of the ESR spectrometer,[23] respectively.

## Results and Discussion

The hypericin salts $\mathbf{Hy}^{-}X^{+}$ are soluble and stable in many organic solvents such as THF, MeCN, or DMF, and also in their mixtures with water. For the less soluble hypericin (**HyH**) which presumably has the structure of the 1,6-tautomer in the solid state, carefully dried THF or DMF must be used to avoid the facile loss of a proton to form $\mathbf{Hy}^{-}$ (**HyH** is only slightly soluble in MeCN). The problem arising from the deprotonation of **HyH** and the lability of its redox stages will be considered in the following sections.

**ESR/ENDOR Spectra.** When $\mathbf{Hy}^{-}Na^{+}$ is reacted with potassium in THF or with zinc in DMF and DMF/$H_2O$ (10:1), the solutions turn from dark to light red and give rise to well-resolved ESR and ENDOR spectra, as exemplified in Figure 1. Identical spectra are observed under the same conditions for $\mathbf{Hy}^{-}X^{+}$ where X is other than Na (X = Cs, $Et_3NH$, lysineH). Irrespective of the nature of X, the intensity of the spectra hardly

(12) Klessinger, M.; Michl, J. *Lichtabsorption und Photochemie organischer Moleküle*; VCH Publishers: Weinheim, Germany, 1989; Chapter 7.6.1. Schuster, G. R. In *Advances in Electron Transfer Chemistry*; Mariano, P. S., Ed.; JAI Press Inc.: Greenwich, CT; Vol. 1, 1991, pp 163–197.

(13) Schreiber, J.; Mottley, C.; Sinha, B. K.; Kayanamaran, B.; Mason, R. P. *J. Am. Chem. Soc.* **1987**, *109*, 348–351. Jülich, T.; Scheffler, K.; Schuler, P.; Stegmann, H .B. *Magn. Reson. Chem.* **1988**, *26*, 701–6. Jülich, T.; Stegmann, H. B.; Krohn, K.; Eickhoff, A. *Magn. Reson. Chem.* **1991**, *29*, 178–83.

(14) Mazur, Y.; Bock, H.; Lavie, D. Canadian Patent Appl. 202993, 1992; *CA* **1992**, *116*, 63432.

(15) Freeman, D.; Frolow, F.; Kapinus, E.; Lavie, G.; Lavie, D.; Meruelo, D.; Mazur, Y. *J. Chem. Soc., Chem. Commun.* **1994**, 891–2.

(16) Etzlstorfer, C.; Falk, H.; Oberreiter, M. *Monatsh. Chem.* **1993**, *124*, 923–9. Mazur, Y. and co-workers. In preparation. See also: Gai, F.; Fehr, M. J.; Petrich, J. W. *J. Phys. Chem.* **1994**, *98*, 5784–95.

(17) Ohya-Nishiguchi, H. *Bull. Chem. Soc. Jpn.* **1979**, *52*, 2064–8.

(18) Kurreck, H.; Kirste, B.; Lubitz, W. *Electron Nuclear Double Resonance Spectroscopy of Radicals in Solution;* VCH Publishers: New York, 1988; Chapter 2.

(19) Kirste, B. *Anal. Chim. Acta* **1992**, *265*, 191–200.

(20) For further details, see: Salbeck, J. Dissertation, Universität of Regensburg, 1988.

(21) Ferrocen: $E_{1/2}$ = 0.326 V; see: Bard, A. J.; Faulkner, L. R. *Electrochemical Methods: Fundamentals and Applications*; Wiley: New York, 1980; pp 699 and 701.

(22) Salbeck, J. *Anal. Chem.* **1993**, *65*, 2169–73.

(23) Gescheidt, G. *Rev. Sci. Instrum.* **1994**, *65*, 2145–6.

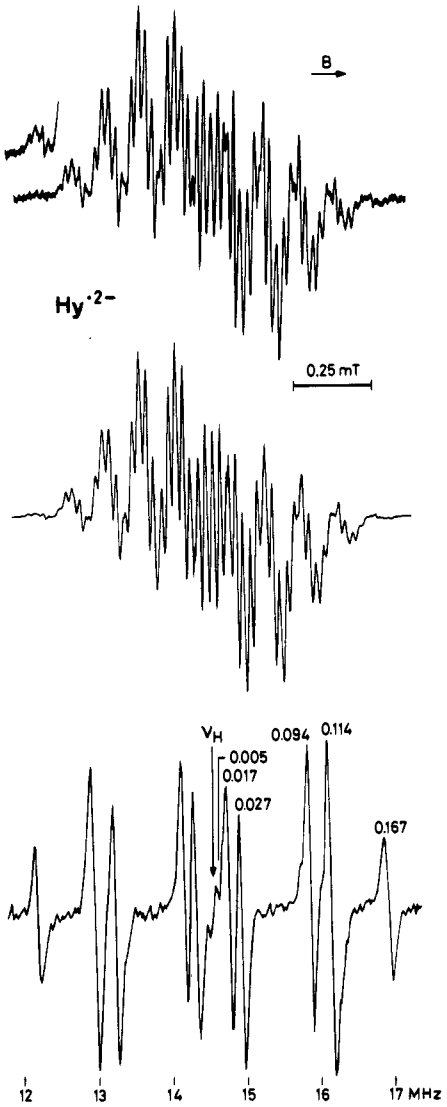


**Figure 1.** Top: ESR spectrum of $\mathbf{Hy}^{\bullet 2-}$. Solvent, THF; counterions, $Na^+$ and $K^+$; temperature, 298 K. Center: simulation of the ESR spectrum. Coupling constants given in Table 1; line shape, Lorentzian; line width, 0.018 mT. Bottom: corresponding proton-ENDOR spectrum at 243 K. The numbers are the coupling constants (absolute values in mT) associated with the signals.

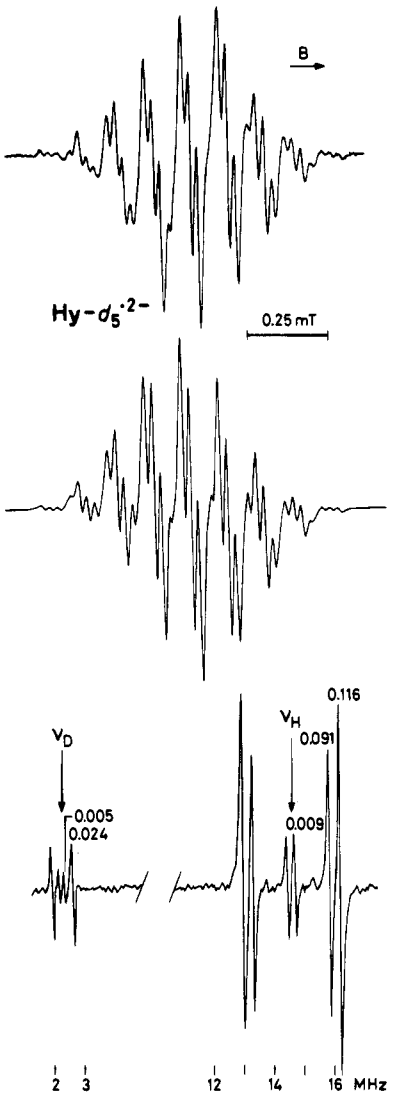


**Figure 2.** Top: ESR spectrum of $\mathbf{Hy}$-$d_5^{\bullet 2-}$. Solvent, DMF-$d_8$/$D_2O$ (10:1); counterions, $Na^+$ and $Zn^{2+}$; temperature, 298 K. Center: simulation of the ESR spectrum. Coupling constants given in Table 1; line shape, Lorentzian; line width, 0.025 mT. Bottom: corresponding proton- (right) and deuteron-ENDOR spectra (left) at 243 K. The numbers are the coupling constants (absolute values in mT) associated with the signals.

decreases over a period of several weeks, even at room temperature, thus pointing to a high persistence of the paramagnetic species in question. The same ESR spectra are also obtained upon electrolysis of $\mathbf{Hy}^-X^+$. The observed ESR and ENDOR spectra must undoubtedly be attributed to the one-electron reduction product of $\mathbf{Hy}^-$, the radical dianion $\mathbf{Hy}^{\bullet 2-}$, of which the interaction with the counterions is not detectable.

Table 1 lists the coupling constants $a_H$ for $\mathbf{Hy}^{\bullet 2-}$ generated from $\mathbf{Hy}^-$ under various conditions. Except for the largest $a_H$ value due to an odd proton, all coupling constants involve sets with even numbers of protons and reflect an effective $C_2$ symmetry. Assignments to protons in individual positions are straightforward for the two largest $a_H$ values, +0.167 and +0.114 mT, arising from the single proton in the 3- or 4-OH group and the six protons of the two 10,11-methyl substituents, respectively. The four smaller $a_H$ values, due to pairs of protons, can partly be assigned by a H/D exchange, as described below. Relative signs of the coupling constants have been determined by a general-TRIPLE resonance experiment;[18] the absolute ones are based on the reasonable assumption that the $a_H$ value of the six $\beta$-methyl protons[24] is positive.

Figure 2 shows the ESR and ENDOR spectra observed upon reaction of $\mathbf{Hy}^-Na^+$ with zinc in DMF-$d_8$/$D_2O$ (10:1). The coupling constants of protons and deuterons, $a_H$ and $a_D$, obtained therefrom are also given in Table 1. It is obvious that of the six $a_H$ values measured with DMF/$H_2O$ only three (+0.116, −0.090, and −0.010 mT) are still observable; the remaining three (+0.157, −0.029, and −0.015 mT) have been replaced by the corresponding $a_D$ values (+0.024, −0.005, and −0.002 mT). As expected, the six $\beta$-protons of the two methyl substituents and the two pairs of α-protons[24] at the four carbon $\pi$-centers do not undergo a H/D exchange, whereas the single proton and the two pairs of protons in the OH groups are substituted by deuterons. The paramagnetic species giving rise to the ESR and ENDOR spectra is thus the pentadeuterated radical dianion $\mathbf{Hy}$-$d_5^{\bullet 2-}$ and, consequently, −0.029 and −0.015 mT must be assigned to the exchangeable protons in the 1,6- and 8,13-OH groups of $\mathbf{Hy}^{\bullet 2-}$, leaving −0.090 and −0.010 mT for the α-protons in the unsubstituted 2,5- and 9,12-positions. More detailed assignments within the two pairs of α-protons

(24) In ESR spectroscopy, protons separated from a $\pi$-center by 0, 1, 2, ... $sp^3$-hybridized carbon atoms are denoted α, $\beta$, $\gamma$, .... In general, coupling constants of α-protons are negative, while those of $\beta$-protons have a positive sign (see, e.g.: Gerson, F. *High-Resolution ESR Spectroscopy*; J. Wiley and Verlag Chemie: New York and Weinheim, F.R.G., 1970; Chapter 1.5.

**Table 1.** Proton- and Deuteron-Coupling Constants, $a_H$ and $a_D$ in mT,[a] for **Hy**$^{\bullet 2-}$, **Hy**-$d_5^{\bullet 2-}$, and [**HyH**]$^{\bullet -}$

| **Hy**$^{\bullet 2-}$ | | | **Hy**-$d_5^{\bullet 2-}$ | [**HyH**]$^{\bullet -}$ | | |
|---|---|---|---|---|---|---|
| THF; $X^+$,[b] $K^+$ | DMF; $X^+$,[b] $Zn^{2+}$ | DMF/$H_2O$; $Na^+$, $Zn^{2+}$ | DMF-$d_8$/$D_2O$; $Na^+$, $Zn^{2+}$ | THF; $K^+$ | DMF; $Zn^{2+}$ | assignment |
| +0.167 (1H) | +0.160 | +0.157 | +0.024 (1D) | −0.059 (2H) | −0.056 | 3,4-OH |
| +0.114 (6H) | +0.115 | +0.116 | +0.116 (6H) | +0.119 (6H) | +0.121 | 10,11-$CH_3(\beta)$ |
| −0.094 (2H) | −0.093 | −0.090 | −0.091 (2H) | −0.091 (2H) | −0.087 | 2,5 or 9,12(α) |
| −0.027 (2H) | −0.028 | −0.029 | −0.005 (2D) | −0.026 (2H) | −0.026 | 1,6- or 8,13-OH |
| −0.017 (2H) | −0.016 | −0.015 | −0.002 (2D)[c] | −0.026 (2H) | −0.026 | 1,6- or 8,13-OH |
| −0.005 (2H)[d] | −0.006[d] | −0.010 | −0.009 (2H) | −0.005 (2H)[d] | −0.005[d] | 2,5 or 9,12(α) |

[a] Experimental error in $a_H$ and $a_D$: ±0.001 mT; $g$ = 2.00275 ± 0.00005, throughout. Conditions: solvent; counterion. [b] X = Na, Cs, $Et_3NH$, lysineH. [c] Too small to be observed; expected by the relation $a_D = 0.1535a_H$. [d] Sign not verified experimentally; assumed by analogy with the corresponding values observed with DMF/$H_2O$ and DMF-$d_8$/$D_2O$.

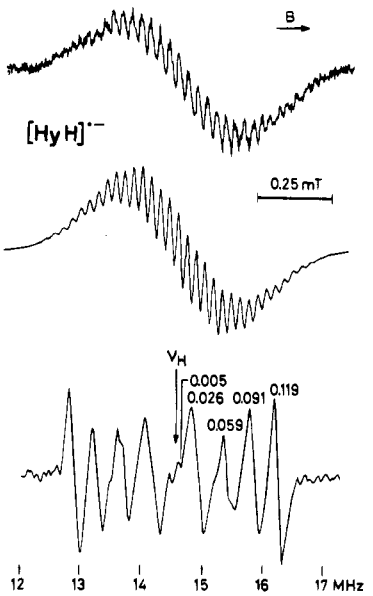


**Figure 3.** Top: ESR spectrum of [**HyH**]$^{\bullet -}$. Solvent, THF; counterion, $K^+$; temperature, 298 K. Center: simulation of the ESR spectrum. Coupling constants given in Table 1; line shape, Lorentzian; line width, 0.050 mT. Bottom: corresponding proton-ENDOR spectrum at 243 K. The numbers are the coupling constants (absolute values in mT) associated with the signals.

and those of the OH protons require further experimental and/or theoretical information which is not available at present.[25]

When the solution of **Hy**$^{\bullet 2-}$ is brought into prolonged contact with the potassium metal in THF, the ESR spectrum of the radical dianion disappears, along with a simultaneous change of color from red to green. Evidently, reduction of **Hy**$^{\bullet 2-}$ to the diamagnetic trianion **Hy**$^{3-}$ then occurs. No new ESR signals are detected even upon exhaustive electrolysis or after the solution has been left standing over the metal mirror at 195 K for 2 weeks.

Reaction of **HyH** with potassium in THF or with zinc in DMF under strictly anhydrous conditions leads to a poorly resolved ESR spectrum which is distinctly different from that of **Hy**$^{\bullet 2-}$; its analysis relies on the observation of well-defined proton-ENDOR signals. Figure 3 shows the pertinent ESR and ENDOR spectra, while the coupling constants $a_H$ determined therefrom are given in Table 1. They clearly identify the paramagnetic species in question as the radical anion [**HyH**]$^{\bullet -}$ with two non-dissociated 3,4-OH groups as the prominent coupling constant of the odd proton is missing.

A straightforward assignment can only be made for the coupling constant of the six methyl $\beta$-protons ($a_H$ +0.119 mT). A positive sign of this value, together with the information provided by the general-TRIPLE-resonance spectrum of [**HyH**]$^{\bullet -}$, demands that other coupling constants, all due to pairs of protons, must be negative. Because of the strictly anhydrous conditions required for the formation of [**HyH**]$^{\bullet -}$, an exchange of OH protons for deuterons with $D_2O$ could not be used to differentiate between the $a_H$ values of these protons and those of α-protons, as in the case of **Hy**$^{\bullet 2-}$.[29] However, all but one of the coupling constants for [**HyH**]$^{\bullet -}$ are so similar to the corresponding values for **Hy**$^{\bullet 2-}$ that distinction between the two sorts of protons has been made by comparison of the former with the latter (Table 1). The only $a_H$ value, −0.059 mT, of a pair of protons in [**HyH**]$^{\bullet -}$ that has no counterpart in **Hy**$^{\bullet 2-}$ must be assigned to the two equivalent protons in the non-dissociated 3,4-OH groups; it replaces the coupling constant, +0.167 mT, observed for a single proton in **Hy**$^{\bullet 2-}$.

The radical anion [**HyH**]$^{\bullet -}$ has rather a low persistence because its ESR and ENDOR spectra (Figure 3) are superseded within a few minutes by those of **Hy**$^{\bullet 2-}$ (Figure 1). The rate of this formal deprotonation (or, more realistically, loss of a hydrogen atom to yield **Hy**$^-$ and subsequent reduction to **Hy**$^{\bullet 2-}$) varies from one experiment to another, depending on such factors as traces of water and duration of the reaction with the reducing agent. Upon prolonged contact of the solution in THF with the potassium mirror, the same reaction path is followed as that described above for **Hy**$^{\bullet 2-}$ starting from **Hy**$^-X^+$.

$$\mathbf{HyH} \xrightarrow{+e^-} [\mathbf{HyH}]^{\bullet -} \xrightarrow{-H} \mathbf{Hy}^- \xrightarrow{+e^-} \mathbf{Hy}^{\bullet 2-} \xrightarrow{+e^-} \mathbf{Hy}^{3-}$$

**Electrochemistry**. Figure 4 shows cyclic voltammograms of **Hy**$^-Na^+$ in MeCN. With a hanging mercury-drop working electrode and glassy carbon counter electrode, three reversible waves, of which the shape does not depend on the scan rate, appear at the potentials $E_{1/2}^{(1)} = -1.12$ V, $E_{1/2}^{(2)} = -1.44$ V, and $E_{1/2}^{(3)} = -1.97$ V *vs* Ag/AgCl (Figure 4a). On the other hand, with a platinum-disk working electrode and platinum-wire counter electrode, only the two first reversible waves are detected at virtually unchanged potentials $E_{1/2}^{(1)}$ and $E_{1/2}^{(2)}$ (Figure 4b); the third wave is not discernible because the current rises drastically above −1.9 V. All these waves can also be observed under the same conditions for **Hy**$^-X^+$, where X = Na is replaced by Cs, $Et_3NH$, or lysineH, and when DMF or MeCN/$H_2O$ (10:1) is used instead of MeCN. Table 2 lists the $E_{1/2}$

(25) Comparison of the experimentally found proton-coupling constants with those calculated by Hückel-McLachlan,[26] AM1,[27] or INDO procedures[28] (using the conventional parameters) has not proven very informative for assignments of the coupling constants. This result is not surprising in view of the large size of the molecular $\pi$-system, its helical geometry comprising several hydrogen bridges, and, last but not least, the small magnitude of the $a_H$ values in question.

(26) McLachlan, A. D. *Mol. Phys.* **1960**, *3*, 233−52.

(27) Dewar, M. J. S.; Zoebisch, E. G.; Healy, E. F.; Stewart, J. J. P. *J. Am. Chem. Soc.* **1985**, *107*, 3902−9. For conversion of 1s-spin populations at hydrogen atoms into coupling constants of α- and $\beta$-protons see: Nelsen, S. F. *J. Chem. Soc., Perkin Trans. 2*, **1988**, 1005−8.

(28) Pople, J. A.; Beveridge, D. L. *Approximate Molecular Orbital Theory*; McGraw-Hill: New York, 1970.

(29) Use of **HyH**-$d_6$ as the starting material, in which all six OH protons were replaced by deuterons, and with anhydrous THF-$d_8$ as the solvent, led to the same results as those obtained with the undeuterated compound **HyH**. Evidently, even in THF-$d_8$, a rapid H−D exchange, due to a minute trace of protic impurities, could not be avoided.

**Table 2.** Reduction Potentials, in V vs Ag/AgCl,[a] of $\mathbf{Hy}^{-}X^{+}$ and **HyH** in Different Solvents

| | $Hy^{-}Na^{+}$ | | | $\mathbf{Hy}^{-}Cs^{+}$ | $\mathbf{Hy}^{-}Et_3NH^{+}$ | $\mathbf{Hy}^{-}$lysineH$^{+}$ | | **HyH** | | |
|---|---|---|---|---|---|---|---|---|---|---|
| | MeCN[b] | DMF[b] | THF[c] | MeCN[b] | MeCN[b] | MeCN[b] | MeCN/$H_2O$[b] | DMF[c] | THF[c] | THF[d] |
| $E_{pc}/E_{pa}$ | | | | | | | | −0.66/−0.52 | −0.63/−0.19 | −0.90 |
| $E_{1/2}^{(1)}$ | −1.12 | −1.14 | −1.26 | −1.11 | −1.15 | −1.11 | −1.04 | −1.14 | −1.26 | −1.28 |
| $E_{1/2}^{(2)}$ | −1.44 | −1.53 | −1.64 | −1.42 | −1.45 | −1.42 | −1.21 | −1.53 | −1.64 | −1.61 |
| $E_{1/2}^{(3)}$ | −1.97 | −2.18 | | −1.98 | −1.97 | −2.0±0.1 | −1.6±0.1 | | | |

[a] Calibrated *vs* ferrocene/ferrocene$^{+}$ and adapted to Ag/AgCl by adding +0.33 V.[21] Error in measurement: ±0.02 V unless indicated otherwise; see Experimental Section for conditions. [b] Working electrode, hanging mercury drop; counter electrode, glassy carbon. [c] Working electrode, platinum disk; counter electrode, platinum wire. [d] Working electrode, glassy carbon; counter electrode, glassy carbon.

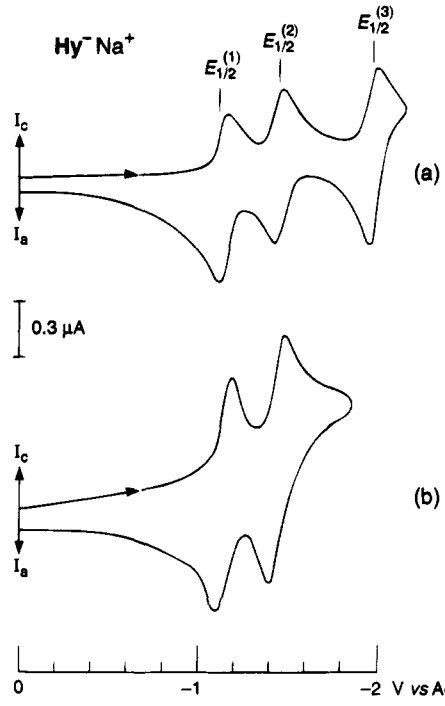


**Figure 4.** Cyclic voltammograms of $\mathbf{Hy}^{-}Na^{+}$. $I_c$ = cathodic; $I_a$ = anodic current; solvent, MeCN; supporting electrolyte, *n*-$Bu_4NClO_4$; temperature, 298 K; scan rate 0.250 V/s: (a) working electrode, hanging mercury drop; counter electrode, glassy carbon; (b) working electrode, platinum disk; counter electrode, platinum wire.

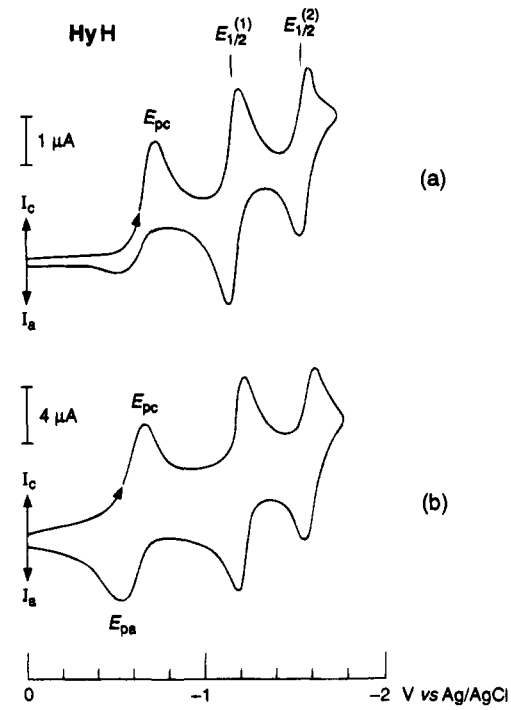


**Figure 5.** Cyclic voltammograms of **HyH**. $I_c$ = cathodic; $I_a$ = anodic current; solvent, DMF; supporting electrolyte, *n*-$Bu_4NPF_6$; temperature, 298 K; working electrode, platinum disk; counter electrode, platinum wire; scan rate 0.025 (a) and 0.250 V/s (b).

values of $\mathbf{Hy}^{-}X^{+}$ for various counterions $X^{+}$ and in several solvents. While these values are rather insensitive to the nature of $X^{+}$, they clearly respond to the change in the medium. The less polar the solvent is, the harder it is to reduce the salts $\mathbf{Hy}^{-}X^{+}$.

The two waves at $E_{1/2}^{(1)}$ and $E_{1/2}^{(2)}$ are attributed to the redox steps $\mathbf{Hy}^{-}/\mathbf{Hy}^{\bullet 2-}$ and $\mathbf{Hy}^{\bullet 2-}/\mathbf{Hy}^{3-}$, respectively. They occur in the range characteristic of quinones such as anthra-9,10-dione[30] but the difference $|E_{1/2}^{(2)} - E_{1/2}^{(1)}|$ of 0.3 ± 0.1 V is distinctly smaller than the corresponding value for quinones (0.7 V for anthra-9,10-dione). This finding points to a weaker interaction between the relevant CO groups in the helically twisted $\mathbf{Hy}^{-}$ (see below) than in the planar and less extended quinones. Thus, the two reduction potentials of $\mathbf{Hy}^{-}$ are compatible with a biphenoquinone being the redox-active moiety of its $\pi$-system. The third wave at $E_{1/2}^{(3)}$, observed only with the hanging mercury drop as the working electrode, should imply a redox step $\mathbf{Hy}^{3-}/\mathbf{Hy}^{\bullet 4-}$.[31] Such a step is conceivable in view of the extended $\pi$-system of $\mathbf{Hy}^{-}$ which ought to accept several additional electrons.

The cyclic voltammograms of **HyH** in carefully dried DMF, obtained with the platinum electrodes, are displayed in Figure 5. They exhibit a quasi-reversible reduction wave at a substantially less negative potential, $E_{pc}$ = −0.66 V *vs* Ag/AgCl, in addition to those observed for $\mathbf{Hy}^{-}X^{+}$. The shape, the potential, and the occurrence of this wave clearly depend on the scan rate (Figure 5), the solvent, and the nature of the working electrode. When DMF is replaced by THF as the solvent, the additional wave is also apparent but remains almost irreversible even at an enhanced scan rate. With glassy carbon as the working electrode, the peak at $E_{pc}$ is shifted to −0.90 V and, with a gold or a hanging mercury-drop electrode, no such wave can be detected. The two subsequent reversible waves, of which the potential does not drastically shift with solvent and the electrode material, closely resemble those of $\mathbf{Hy}^{-}X^{+}$ at the potentials $E_{1/2}^{(1)}$ and $E_{1/2}^{(2)}$.[32] All values pertinent to **HyH** in both DMF and THF are included in Table 2.

The characteristic behavior of the additional wave at the potential $E_{pc}$ strongly suggests that this wave has to be ascribed to the reduction of an acidic proton, C(3)−OH or C(4)−OH, at the electrode surface.[33] The least negative potential for $E_{pc}$ has

(30) Meites, L.; Zuman, P.; Rupp, E. B.; Fenner, T. L.; Narayanan, A. *CRC Handbook; Series in Organic Chemistry;* CRS Press: West Palm Beach, 1978; Vol. III.

(31) This redox wave at $E_{1/2}^{(3)}$ is distinct only when the cyclic voltammogram is recorded immediately after the generation of a "fresh" mercury drop; upon leaving such a drop hanging for ca. 1 min, the wave becomes masked by other signals, presumably due to adsorption processes. The finding that, with a platinum disk as the working electrode, the current is strongly enhanced above −1.9 V, thus impairing the measurement of redox waves at a more negative potential, points likewise to an adsorption of $\mathbf{Hy}^{-}Na^{+}$ at the electrode.

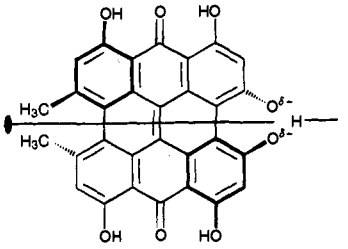

**Figure 6.** Geometry of $\mathbf{Hy}^-$ as indicated by theoretical calculations and supported by the X-ray crystallographic structure analysis of $\mathbf{Hy}^-$ pyridineH$^+$.[15]

thus been detected at the platinum surface which possesses particular affinity for hydrogen atoms; on the other hand, for the glassy carbon, the gold, and the mercury electrodes, with no preference for such atoms, the wave attributed to $E_{pc}$ is either shifted to more negative potential or not detectable, due to the overpotential for proton reduction at the surfaces of these electrodes. The finding that the reversibility of the wave at $E_{pc}$ is more pronounced in DMF than in the more basic solvent THF also supports its ascription to the reduction of a proton. Thereby, **HyH** is deprotonated to $\mathbf{Hy}^-$ which is subsequently reduced at $E^{(1)}_{1/2}$ to $\mathbf{Hy}^{\bullet 2-}$. This mechanism complies with the observation that the ESR spectrum of $[\mathbf{HyH}]^{\bullet -}$ is replaced by that of $\mathbf{Hy}^{\bullet 2-}$ within a few minutes. The pathways between the redox stages of **HyH** and $\mathbf{Hy}^-$ are outlined below; the last step from $\mathbf{Hy}^{3-}$ to $\mathbf{Hy}^{\bullet 4-}$, which is not fully secured by all experiments, is presented by dashed arrows.[34]

$$\mathbf{HyH} \overset{+e^-}{\rightleftharpoons} (\mathrm{H{\bullet}Pt}) + \mathbf{Hy}^- \underset{-e^-}{\overset{+e^-}{\rightleftharpoons}} \mathbf{Hy}^{\bullet 2-} \underset{-e^-}{\overset{+e^-}{\rightleftharpoons}} \mathbf{Hy}^{3-} \underset{-e^-}{\overset{+e^-}{\rightleftharpoons}} \mathbf{Hy}^{\bullet 4-}$$

**Structures of $\mathbf{Hy}^{\bullet 2-}$ and $[\mathbf{HyH}]^{\bullet -}$.** Molecular mechanics[35] and AM1 calculations[27] point to helically twisted skeletons of hypericin (**HyH**) and its conjugate base ($\mathbf{Hy}^-$), owing to the steric interference of the two 10,11-methyl substituents. This geometry is consistent with the $C_2$ symmetry, whereby the odd hydrogen atom in $\mathbf{Hy}^-$ resides on the 2-fold axis in a symmetric C(3)$-O^{\delta-}\cdots H\cdots{}^{\delta-}$O$-$C(4) bridge (Figure 6). Experimental evidence for such a structure has recently been provided by an X-ray crystallographic analysis of the salt $\mathbf{Hy}^-$ pyridineH$^+$.[15,36] As stated in the previous section, an effective $C_2$ symmetry is also indicated for $\mathbf{Hy}^{\bullet 2-}$ by its hyperfine data. Evidently, the odd hydrogen atom in the C(3)$-O^{\delta-}\cdots H\cdots{}^{\delta-}$O$-$C(4) bridge and the two pairs of hydrogen atoms in the four (presumably) non-symmetric C(1,6)$-$O$-$H$\cdots$O=C(14,7) and C(8,13)$-$O$-$H$\cdots$O=C(7,14) bridges must behave in such a way that the 2-fold axis is not affected on the hyperfine time scale. Moreover, the similarity of all but one of the proton-coupling constants for $[\mathbf{HyH}]^{\bullet -}$ with those for $\mathbf{Hy}^{\bullet 2-}$ testifies that the structures of the two paramagnetic species do not essentially differ. The replacement of the symmetric hydrogen bridge by the two non-dissociated 3,4-OH groups, as the prominent change on going from $\mathbf{Hy}^{\bullet 2-}$ to $[\mathbf{HyH}]^{\bullet -}$, has apparently no marked effect on the $\pi$-system and on the $C_2$ symmetry, common to both species.

**Electronic Spectra.** In solvents such as anhydrous DMF or THF, **HyH** gives rise to several absorption bands in the visible region. With THF, the maxima ($\epsilon$ in dm$^3$ mol$^{-1}$ cm$^{-1}$) lie at 455 ($2 \times 10^4$), 540 ($2 \times 10^4$), and 583 nm ($5 \times 10^4$); they have been assigned to the 1,6-tautomer.[16] On passing to $\mathbf{Hy}^-$, the absorption pattern is preserved and, barely, the maxima are bathochromically shifted, as is also observed upon 1,6- $\rightarrow$ 7,14-tautomerization.[16] For $\mathbf{Hy}^-\mathrm{Na}^+$ in THF, they appear at 483 ($10^4$), 554 ($2 \times 10^4$), and 599 nm ($5 \times 10^4$). Upon reduction of $\mathbf{Hy}^-$ to $\mathbf{Hy}^{\bullet 2-}$, characteristic changes in the electronic spectrum occur; most striking is the appearance of long-wave bands at 670, 740, 1000, and 1150 nm. Attribution of these bands to $\mathbf{Hy}^{\bullet 2-}$ is reasonable because their intensity increases with that of the corresponding ESR spectrum and because long-wave bands in the near IR are often found for large $\pi$-radical ions.[37] Further reduction of $\mathbf{Hy}^{\bullet 2-}$ to $\mathbf{Hy}^{3-}$, manifested by the color change from red to green (see above), shifts the first two of these bands to 690 and 750 nm and leads to the disappearance of the absorption above 900 nm. Similar changes as for $\mathbf{Hy}^-$ are observed for **HyH** under the same conditions, but because of the facile conversion of $[\mathbf{HyH}]^{\bullet -}$ to $\mathbf{Hy}^-$, it is difficult to distinguish the bands of $[\mathbf{HyH}]^{\bullet -}$ and $[\mathbf{HyH}]^{2-}$ from those of $\mathbf{Hy}^{\bullet 2-}$ and $\mathbf{Hy}^{3-}$, respectively.[34]

**Concluding Remarks.** Spectroscopic and electrochemical studies described in the present paper establish hypericin and its salts as efficient acceptors of more than one electron and they provide structural details for their first reduction stages. The ease of deprotonation at the 3,4-OH groups in **HyH** to yield $\mathbf{Hy}^-$ and $\mathbf{Hy}^{\bullet 2-}$ finds its counterpart in the facile conversion of the radical anion $[\mathbf{HyH}]^{\bullet -}$ into $\mathbf{Hy}^-$. Likewise, some changes in bond lengths disregarded, the twisted helical geometry and the effective $C_2$ symmetry of the paramagnetic species, $[\mathbf{HyH}]^{\bullet -}$ and $\mathbf{Hy}^{\bullet 2-}$, are shared with their diamagnetic precursors, **HyH** and $\mathbf{Hy}^-$. Further studies on the proton or hydrogen atom transfers between the redox stages of **HyH** and those of its conjugate base $\mathbf{Hy}^-$ are required for a full clarification of such processes which involve formation and breaking of hydrogen bridges and which may be as relevant to the reactivity of hypericin as are the electron transfers. Notwithstanding the problems still to be solved, the information provided by the present studies should contribute to understanding the mechanism of the pharmacological activity of hypericin and its salts.

**Acknowledgment.** This work was supported by the Swiss National Science Foundation, the German Fonds der Chemischen Industrie, and VIMRx Pharmaceuticals Inc., Stamford, CT. G.G. is indebted to the Freiwillige Akademische Gesellschaft, Basel, for a Treubel Scholarship.

JA952243A

(32) After the experimental work pertinent to the present paper had been accomplished, an observation of two reduction waves in the cyclic voltammogram of hypericin in dimethyl sulfoxide ($Me_2SO$) was reported.[9] The interpretation of the half-wave potentials published therein as those of **HyH** must seriously be doubted. In our hands, **HyH** proved only slightly soluble in $Me_2SO$, and the waves in the cyclic voltammograms were barely detectable. In contrast, $\mathbf{Hy}^-\mathrm{Na}^+$ readily dissolves in $Me_2SO$ and gives rise to the cyclic voltammogram presented in that report. This finding is not surprising because under the conditions of the authors' experiment ("the solvent and the supporting salt, $n$-$Bu_4NClO_4$, were used as purchased"), **HyH** clearly deprotonates to $\mathbf{Hy}^-$ and the two observed waves represent the redox steps $\mathbf{Hy}^-/\mathbf{Hy}^{\bullet 2-}$ and $\mathbf{Hy}^{\bullet 2-}/\mathbf{Hy}^{3-}$.

(33) We thank one of the reviewers for suggesting this mechanism (we have formerly ascribed the wave at $E_{pc}$ to the redox step $\mathbf{HyH}/\mathbf{HyH}^{\bullet -}$) and introducing us to the reference (Barrette, W. C., Jr.; Johnson, H. W., Jr.; Sawyer, D. T. *Anal. Chem.* **1984**, *56*, 1890–8), in which the proton reduction is described. We are also indebted to Prof. H. Seiler, University of Basel, and to Prof J. Heinze, University of Freiburg (Germany), for fruitful discussions and suggestions.

(34) The possibility that some **HyH** survives at the redox step $E_{pc}$ and the subsequent steps $[\mathbf{HyH}]^{\bullet -}/[\mathbf{HyH}]^{2-}$ and $[\mathbf{HyH}]^{2-}/[\mathbf{HyH}]^{\bullet 3-}$ coincide with $\mathbf{Hy}^-/\mathbf{Hy}^{\bullet 2-}$ and $\mathbf{Hy}^{\bullet 2-}/\mathbf{Hy}^{3-}$, respectively, cannot be completely ruled out, considering the similar $\pi$-systems of **HyH** and $\mathbf{Hy}^-$.

(35) MM2(QCPE-395) force field with the $\pi$-VESCF routines taken from MP1(QCPE-318), both by Allinger.

(36) Apart from ref 15, another report on the X-ray structure analysis of hypericin crystallized with pyridine was published (Etzlstorfer, C.; Falk, H.; Müller, N.; Schmitzberger, W.; Wagner, U. G. *Monatsh. Chem.* **1993**, *124*, 751–61). In this paper, non-dissociated 3,4-OH groups are preferred to the C(3)$-O^{\delta-}\cdots H\cdots{}^{\delta-}$O$-$C(4) bridge. Such a structure seems not to be compatible with the ease of deprotonation of **HyH**.

(37) Bachmann, R.; Gerson, F.; Gescheidt, G.; Vogel, E. *J. Am. Chem. Soc.* **1992**, *114*, 10855–60; **1993**, *115*, 10286–92.